

Observation of Unusual Slow-Relaxation of the Magnetisation in a Gd-EDTA MRI Contrast Agent

Rebecca J. Holmberg,^a Le Tuan Anh Ho,^b Liviu Ungur,^b Ilia Korobkov,^a Liviu F. Chibotaru,^{*b} and Muralee Murugesu^{*a}

^a Department of Chemistry, University of Ottawa, 10 Marie Curie Private, Ottawa, ON, Canada K1N 6N5. E-mail: m.murugesu@uottawa.ca; Fax: +1 (613) 562 5170, Tel: +1 (613) 562 5800 ext. 2733

^b Theory of Nanomaterials Group and INPAC Institute for Nanoscale Physics and Chemistry, Katholieke Universiteit Leuven, Celestijnenlaan, 200F, 3001 Leuven, Belgium

Supporting Information:

Experimental Section

Materials and Physical Measurements.

All manipulations were performed under aerobic/ambient conditions. All reagents were purchased from the following sources: Alfa Aesar, Acros Organics, Strem Chemicals, and Sigma Aldrich. All reagents were employed without further purification.

Na[Gd(EDTA)(H₂O)₃]_n·5H₂O (Gd-EDTA) Colourless crystals (Figure S1) were prepared by placing Na₂EDTA (0.186 g, 0.5 mmol) and GdCl₃·6H₂O (0.132 g, 0.5 mmol) in water (25 mL). A solution of 1M aq. NaOH was added drop wise to promote ligand solubility. The suspension was stirred and heated to reflux until dissolved. Once dissolved, the solution was filtered and allowed to slow evaporate until crystals formed. In some cases EtOH was layered in order to promote the formation of crystals. Elemental analysis; expected: C 19.61%, H 4.61%, N 4.57%; Found: C 19.79%, H 4.43%, N 4.56%.

Elemental Analysis Elemental analysis was performed at the Laboratoire d'Analyse Élémentaire de l'Université de Montréal.

Infrared Spectrometry Infrared spectra were recorded in the solid state on a Nicolet 6700 FT-IR spectrometer in the 4000-600 cm⁻¹ region.

X-Ray Crystallography Single crystal X-Ray diffraction experiments were performed on a Bruker AXS SMART single crystal diffractometer with a sealed Mo tube APEX II CCD detector, which was used to collect the unit cell and intensity data using graphite Mo-K α radiation ($\lambda = 0.71073 \text{ \AA}$). Data reduction included correction for Lorentz and polarisation effects, with an applied multi-scan absorption correction (SADABS). Crystal structures were

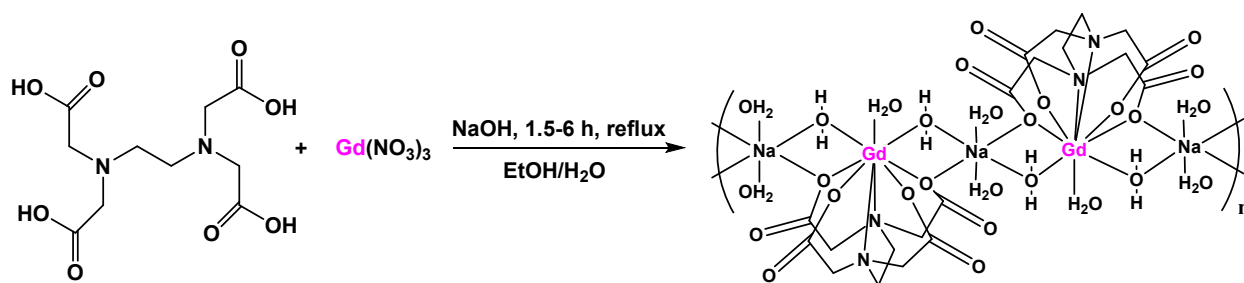
solved and refined using SHELXTL. All non-hydrogen atoms were refined with anisotropic thermal parameters. Hydrogen atom positions were calculated geometrically, and were riding on their respective atoms.

X-ray Powder Diffraction (XRPD) experiments were performed using a RIGAKU Ultima IV, equipped with a Cu-K α radiation source ($\lambda = 1.541836 \text{ \AA}$), and a graphite monochromator. Scanning of the 2θ range was performed from $5-45^\circ$. In order to assign the peaks corresponding to particular crystalline phases, PDXL software equipped with the RIGAKU apparatus was used with the ICDD database. XRPD pattern was consistent in 2θ values with the generated pattern from XRD, with slight discrepancies in some intensities of peaks attributed to preferred orientation.

SEM Scanning electron microscopy (SEM) images were taken of single crystals using a JSM-7500F FESEM (JEOL).

SQUID Magnetic measurements were performed using a Quantum Design SQUID magnetometer MPMS-XL7, operating between 1.8 and 300 K for dc-applied fields ranging from -7 to 7 T. Susceptibility measurements were performed on freshly filtered, crushed crystalline **Gd-EDTA** (22.2 mg), wrapped within a polyethylene membrane. The field dependent magnetisation data of **Gd-EDTA** was also collected at 1.8, 3, 5, and 7 K under applied fields up to 7 T. The magnetisation data were initially collected at 100 K to check for ferromagnetic impurities, found to be absent in all samples. Solution measurements were also performed in order to elicit dilution behaviour, where **Gd-EDTA** (3.5 mg) was dissolved in 0.3 mL H₂O and sealed in a polyethylene casing. After measurements were completed, the solution sample was re-dried and measured for sample weight accuracy. Subsequently, in order to demonstrate that the diamagnetic contribution was not causing the non-superimposition of the curves in M vs. HT⁻¹ solution measurements, we performed a variety of diamagnetic contribution analyses on both the solid and solution samples, as shown in Figures S6 and S10.

Supplemental Figures



Scheme S1: Synthetic scheme highlighting the synthetic conditions and chain structure of **Gd-**

EDTA.

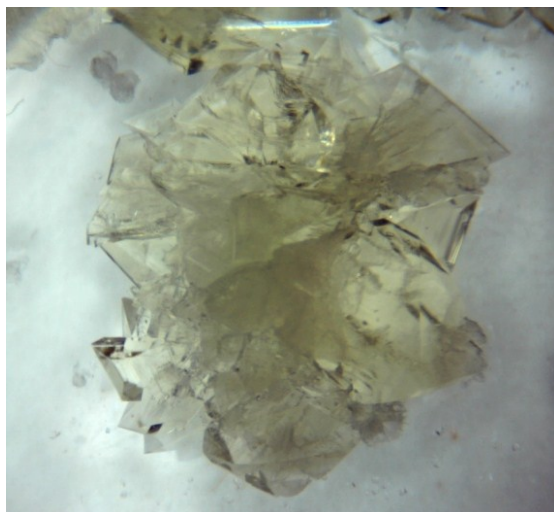


Figure S1. Transparent colourless **Gd-EDTA** crystals observed under a microscope.

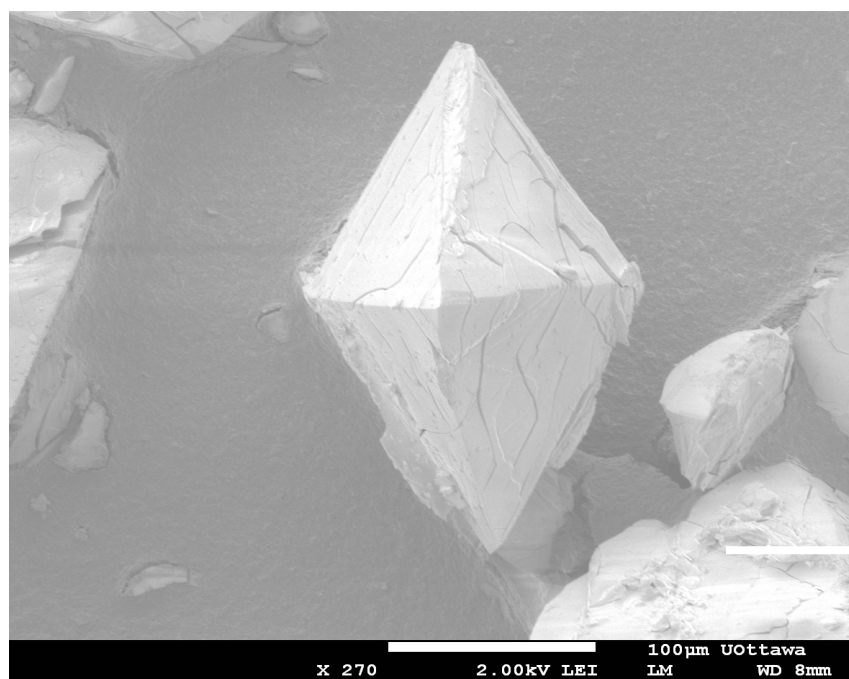


Figure S2. **Gd-EDTA** crystal observed under a scanning electron microscope. Scale bar: 100µm.

Table S1. Crystallographic data for **Gd-EDTA**.

Compound	Gd-EDTA
Empirical formula	C ₁₀ H ₂₈ GdN ₂ NaO ₁₆
Formula weight (g/mol)	612.58
Crystal system	monoclinic
Space group	C c (no. 9)
Temperature (K)	200(2)
Crystal size (mm)	0.24 x 0.19 x 0.16
<i>Z</i>	8
<i>a</i> (Å)	12.0641(4)
<i>b</i> (Å)	19.3270(6)
<i>c</i> (Å)	18.6758(6)
α (°)	90.00
β (°)	108.7327(13)
γ (°)	90.00
Volume (Å ³)	4123.8(2)
Calculated density (gcm ⁻³)	1.973
Absorption coefficient (mm ⁻¹)	3.319
<i>F</i> (000)	2440
θ range for data collection (°)	2.40 – 28.34
Limiting indices	$h = \pm 16, k = \pm 25, l = \pm 24$
Reflections collected/unique	29817/9608
<i>R</i> (int)	0.0216
Completeness to $\theta = 25.242$ (%)	0.997
Max. and min. Transmission	0.6143 and 0.7457
Data/restraints/parameters	9608/2/542
Goodness-of-fit on <i>F</i> ²	1.050
Final <i>R</i> indices [<i>I</i> .2 σ (<i>I</i>)]	$R_1 = 0.0216, wR_2 = 0.0576$
<i>R</i> indices (all data)	$R_1 = 0.0217, wR_2 = 0.0577$
Largest diff. Peak/hole, eÅ ⁻³	0.601 and -0.844

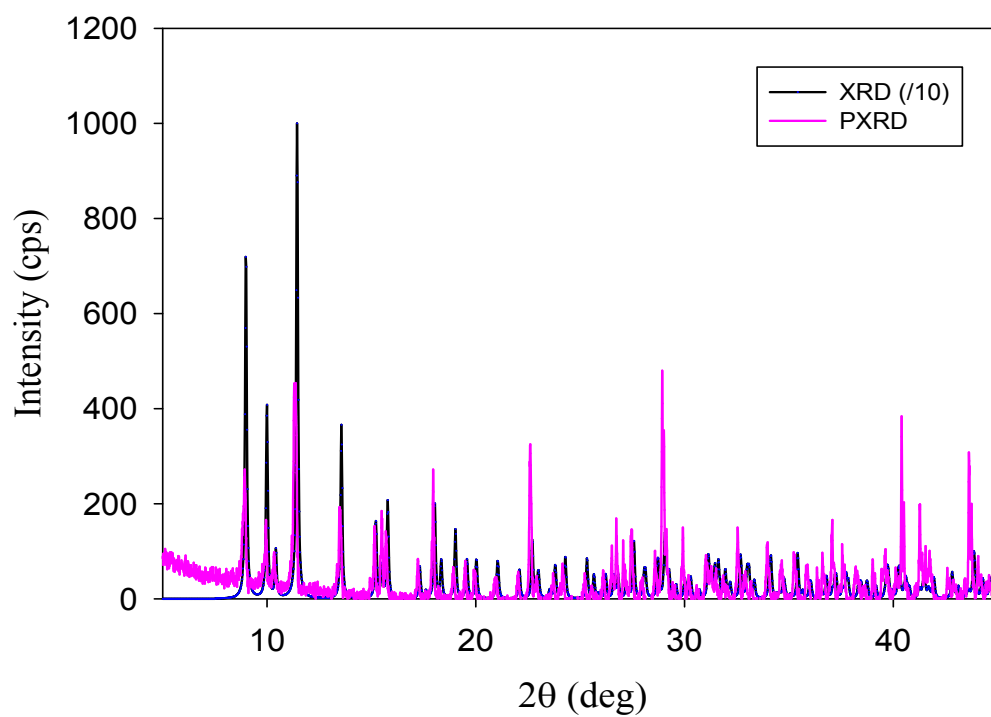


Figure S3. X-ray powder diffraction spectra of **Gd-EDTA** (pink) for air-dried single crystals in the 5-45° 2θ region, as compared with the theoretical pattern generated from single crystal X-ray data (black).

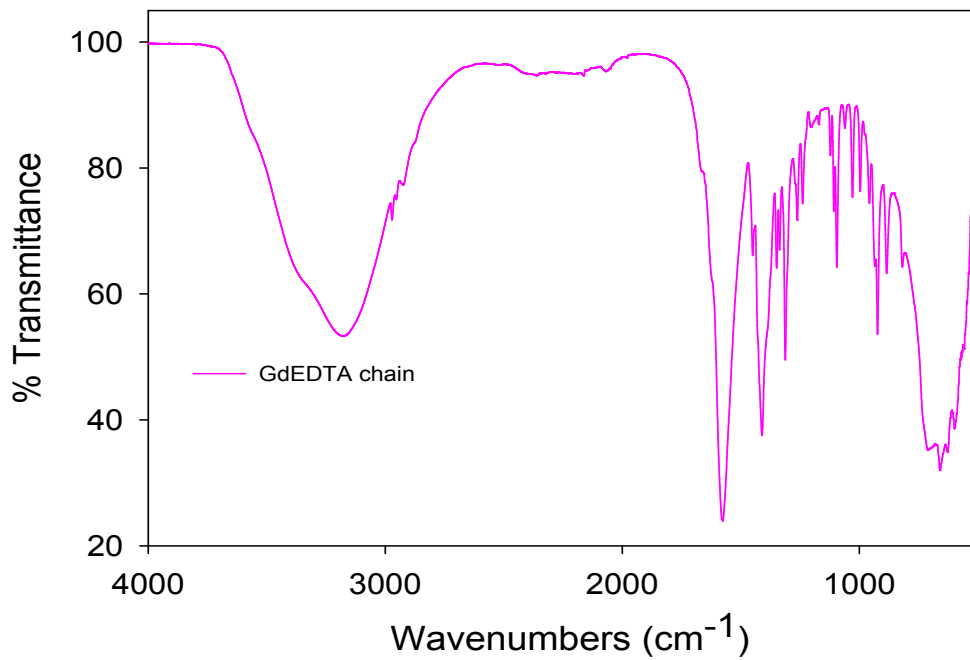


Figure S4. FTIR spectra of **Gd-EDTA** for vacuum filtered crystals in the 4000-600 cm⁻¹ region.

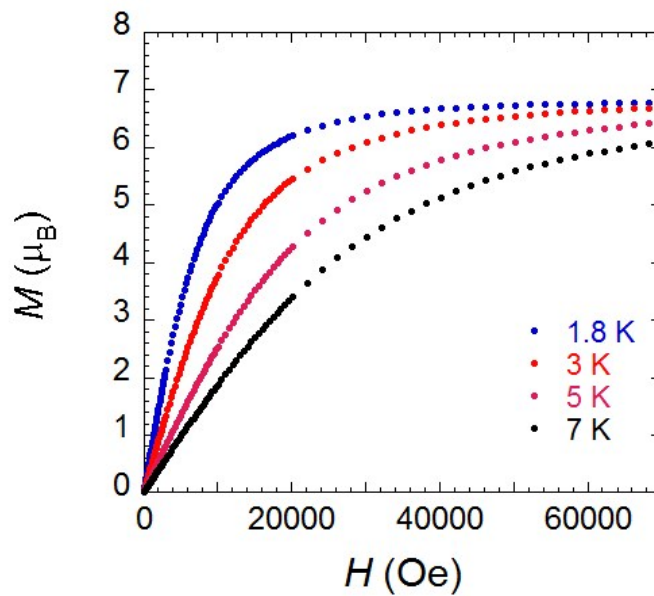


Figure S5. Field dependence of the magnetisation of **Gd-EDTA** at indicated temperatures.

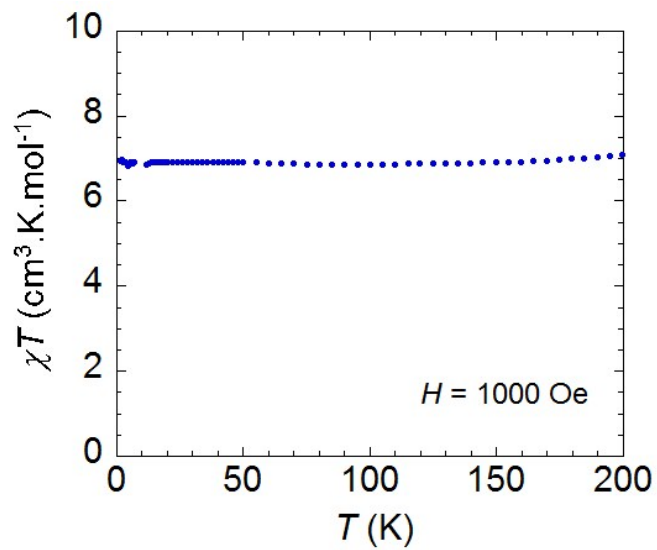


Figure S6. Temperature dependence of the χT product at 1000 Oe for 2 mM **Gd-EDTA** aqueous solution.

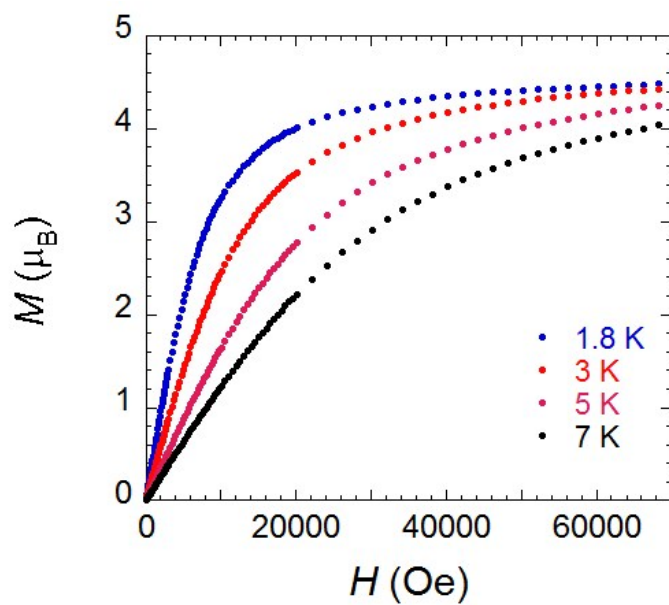


Figure S7. Field dependence of the magnetisation of 2 mM **Gd-EDTA** aqueous solution at indicated temperatures.

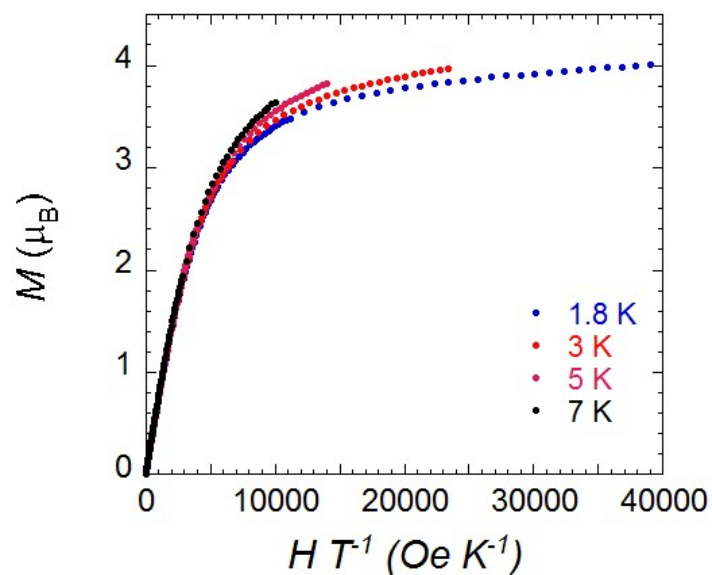


Figure S8. M vs. HT^{-1} plot for 2 mM **Gd-EDTA** aqueous solution at indicated temperatures.

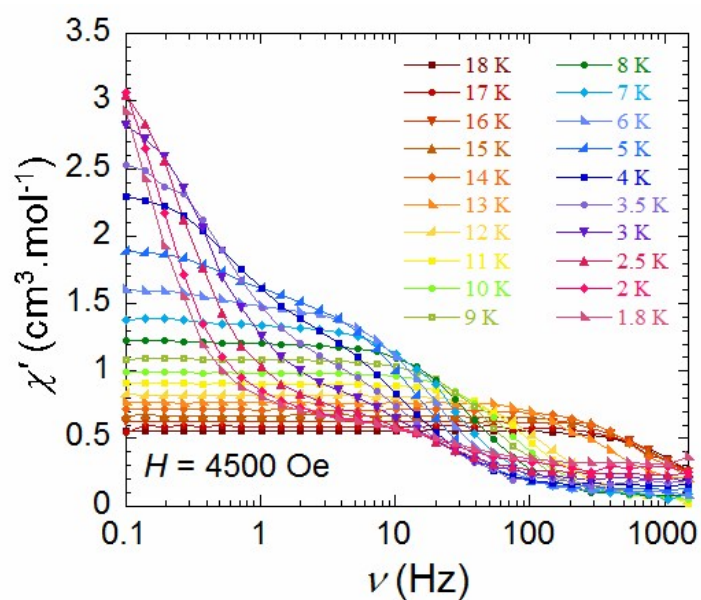


Figure S9. Frequency dependence of the in-phase (χ') susceptibility for **Gd-EDTA** between 1.8 and 18 K under a 4500 Oe applied dc field.

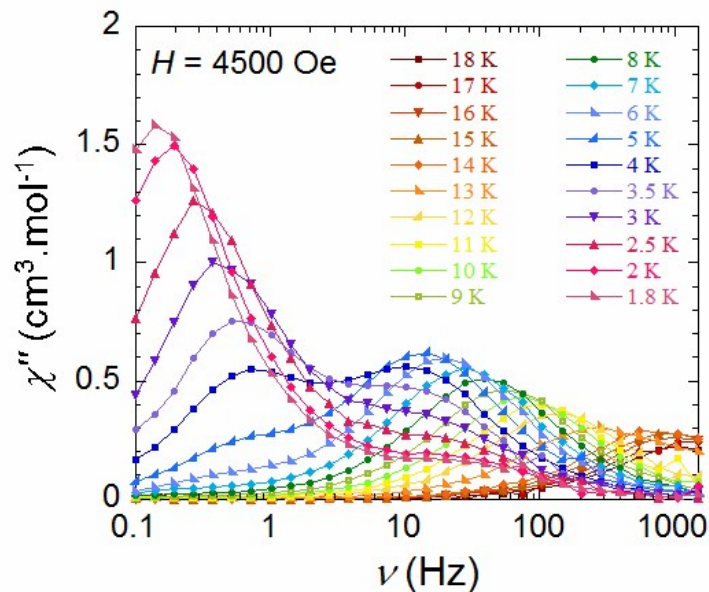


Figure S10. Frequency dependence of the out-of-phase (χ'') susceptibility for **Gd-EDTA** between 1.8 and 18 K under a 4500 Oe applied dc field.

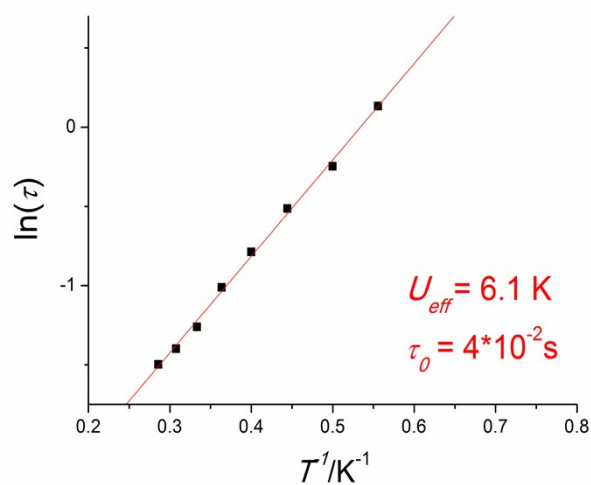


Figure S11. Relaxation time of the magnetization $\ln(\tau)$ vs. T^{-1} for **Gd-EDTA** (Arrhenius plot using ac data) under 4500 Oe applied field (slow relaxation process). The solid red line corresponds to the fit.

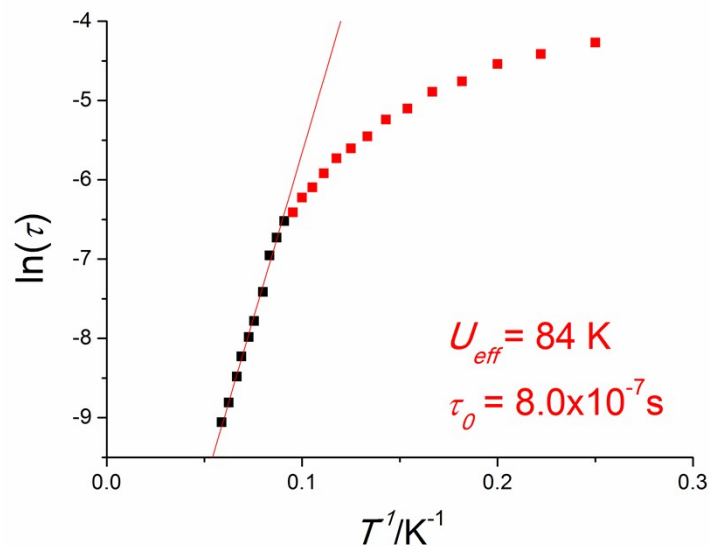


Figure S12. Relaxation time of the magnetization $\ln(\tau)$ vs. T^{-1} for **Gd-EDTA** (Arrhenius plot using ac data) under 4500 Oe applied field (fast relaxation process). The solid red line corresponds to the fit.

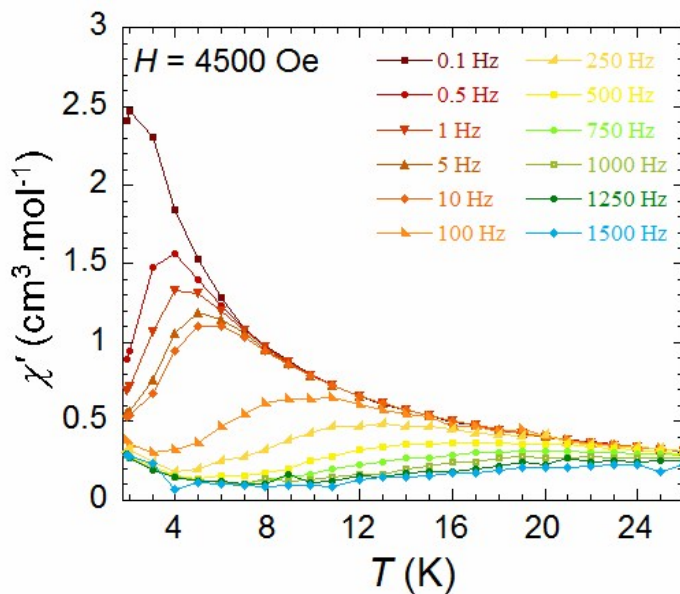


Figure S13. Temperature dependence of the in-phase (χ') susceptibility for **Gd-EDTA** between 0.1 and 1500 Hz under a 4500 Oe applied dc field.

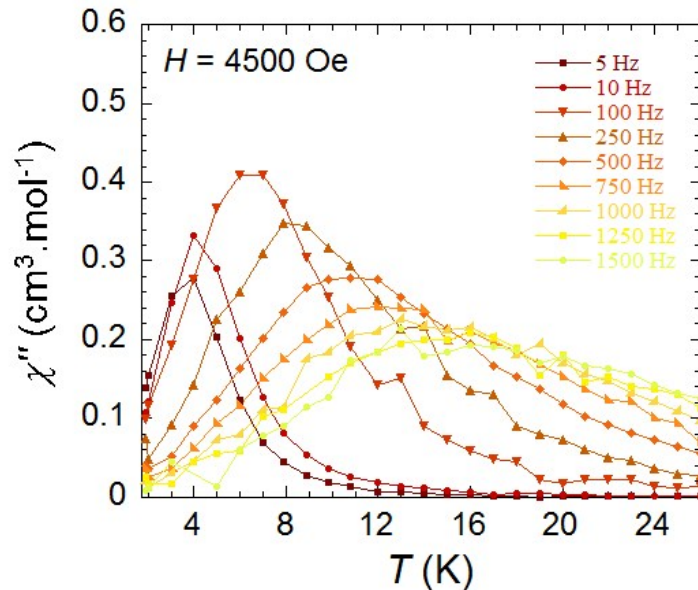


Figure S14. Temperature dependence of the out-of-phase (χ'') susceptibility for **Gd-EDTA** between 0.1 and 1500 Hz under a 4500 Oe applied dc field.

Ab Initio calculations of local anisotropy on Gd sites

All ab initio calculations were done using MOLCAS program package, and were of CASSCF/RASSI/SINGLE_ANISO type.

Three structural fragment models (A, B and C) have been designed to reproduce as accurate as possible the environment of each Gd site. Figure S16-S18 show the structure of the calculated fragments.

Each fragment has been computationally described within three basis set approximations (1, 2 and 3). Table S2 shows the contractions of the employed basis sets. As a result we have calculated each Gd fragment within 7 computational approximations: A1, A2, A3, B1, B2, C1 C2. Computational models B3 and C3 were out of our computational resources.

Table S2. Contractions of the employed ANO-RCC basis sets in all ab initio calculations.

Atom	Basis 1 (minimal)	Basis 2 (DZP)	Basis 3 (TZP)
Gd	ANO-RCC-MB	ANO-RCC-VDZP	ANO-RCC-VTZP
Na		ANO-RCC-VDZP	ANO-RCC-VTZP
O (close)		ANO-RCC-VDZP	ANO-RCC-VTZP

O (distant)		ANO-RCC-MB	ANO-RCC-VDZ
C (close)		ANO-RCC-VDZP	ANO-RCC-VTZP.
C(distant)		ANO-RCC-MB	---
N (close)		ANO-RCC-VDZP	ANO-RCC-VTZP
N (distant)		ANO-RCC-MB	---
H (close)		ANO-RCC-VDZP	ANO-RCC-VTZP
H (distant)		ANO-RCC-MB	ANO-RCC-VDZ

Active space of the CASSCF method included 7 electrons in 7 orbitals. All available spin states were optimized within state-average calculations. Besides the ground 8S state, all spin sextet states (48), 215 spin quartet states (out of 392) and 188 spin doublet states (out of 784) were mixed by the spin-orbit coupling in RASSI. The resulting spin-orbit states are given below (Table S3).

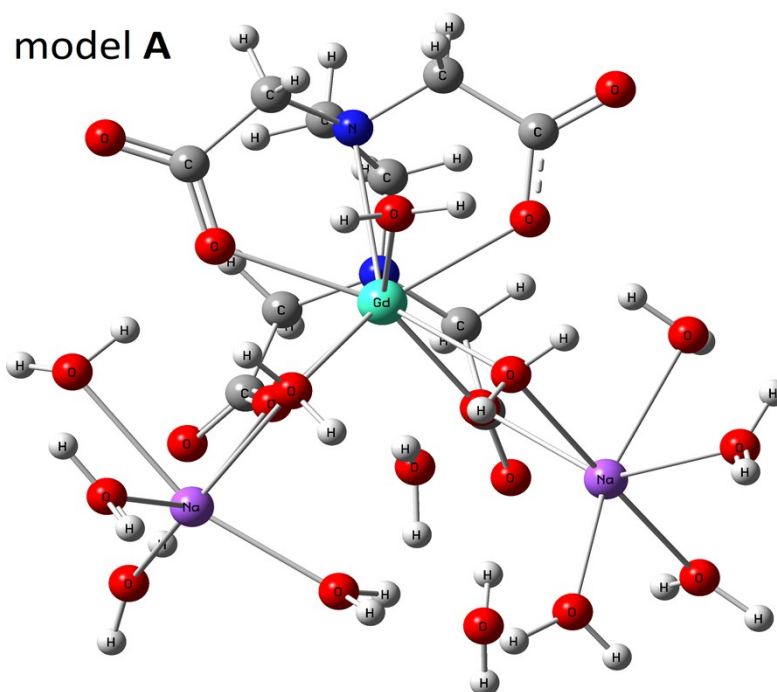


Figure S15. Structure of the calculated model A for the Gd-1 site. Similar structure was employed for Gd-2 site.

model B

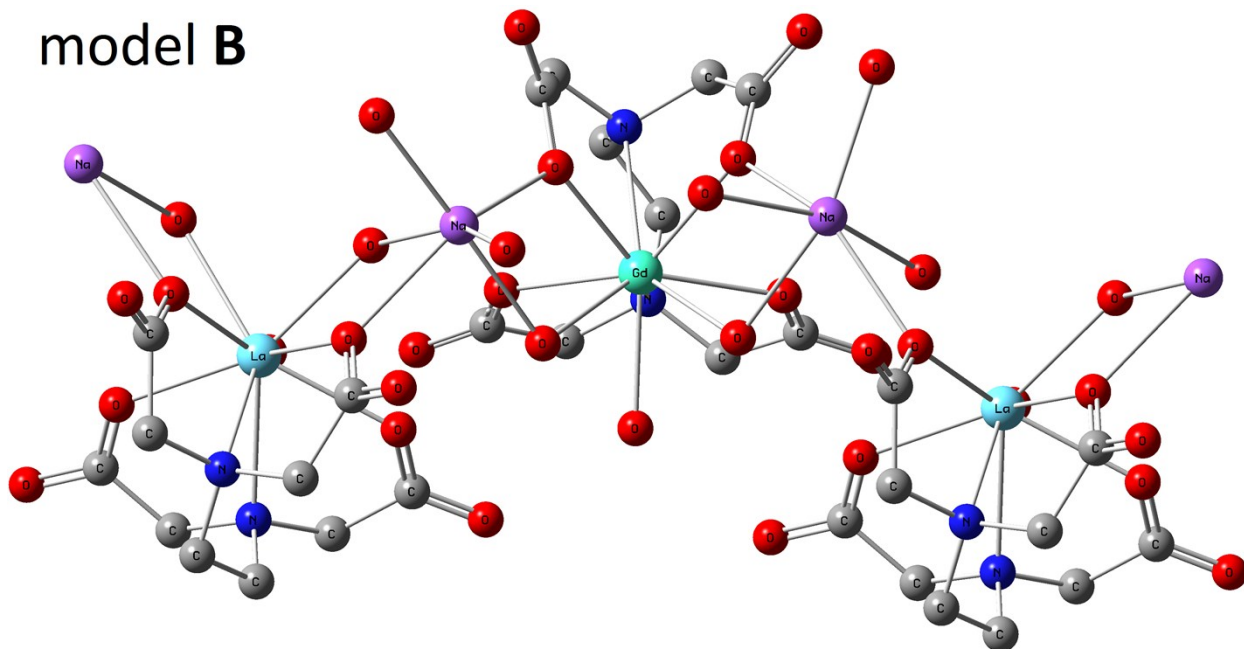


Figure S16. Structure of the calculated model B for the Gd-1 site. Hydrogen atoms are not shown for clarity. No crystalized water is included. Similar structure was employed for Gd-2 site.

model C

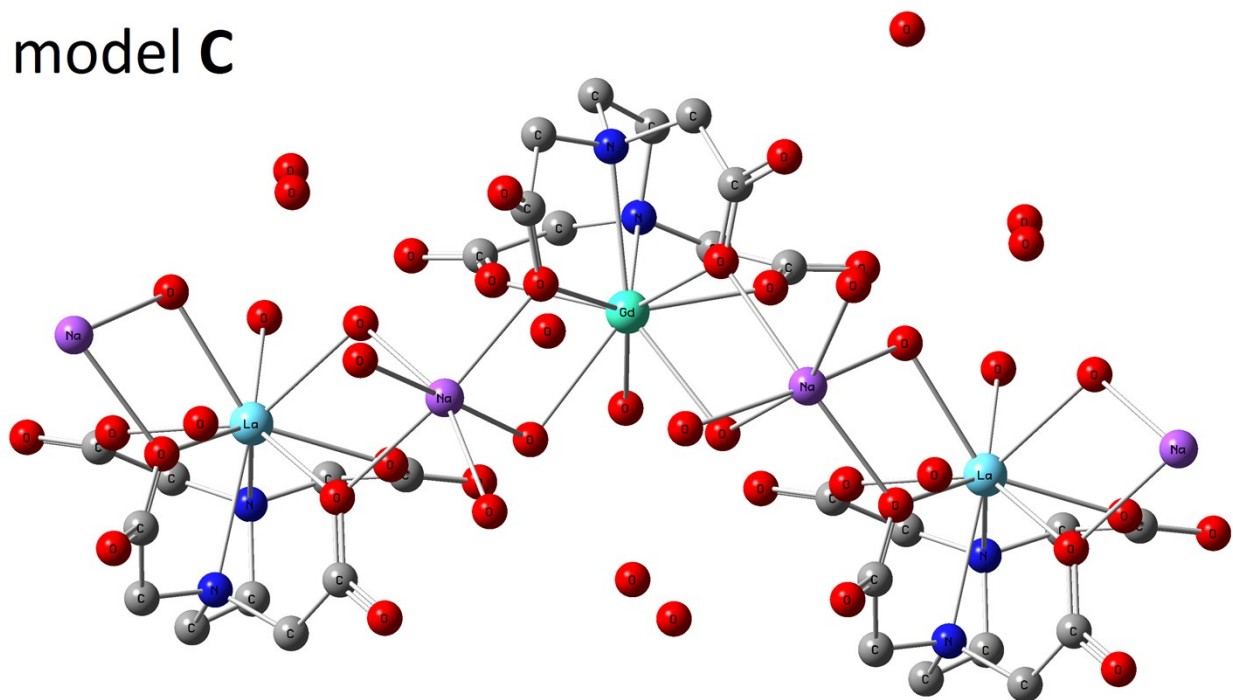


Figure S17. Structure of the calculated model C for the Gd-1 site. Hydrogen atoms are not shown for clarity. Close water molecules were included in the calculation. Similar structure was employed for Gd-2 site.

Table S3. Calculated low-lying spin-orbit energy states for both Gd sites, arising from the zero-field splitting of the ground $S = 7/2$ (in cm^{-1}). Anisotropy parameters D and E are given for the zero-field splitting Hamiltonian: $H_{ZFS} = DS_Z^2 + E(S_X^2 - S_Y^2)$.

model A:

Gd-1			Gd-2		
Basis 1	Basis 2	Basis 3	Basis 1	Basis 2	Basis 3
0.000	0.000	0.000	0.000	0.000	0.000
0.179	0.309	0.269	0.157	0.284	0.253
0.341	0.618	0.536	0.314	0.570	0.494
0.597	1.113	0.961	0.564	1.026	0.879
g tensor for the ground Kramers doublet (highlighted, pseudospin=1/2)					
$g_X = 0.466$	$g_X = 0.588$	$g_X = 0.572$	$g_X = 0.584$	$g_X = 0.588$	$g_X = 0.518$
$g_Y = 0.774$	$g_Y = 1.027$	$g_Y = 0.994$	$g_Y = 1.019$	$g_Y = 1.030$	$g_Y = 0.880$
$g_Z = 13.455$	$g_Z = 13.317$	$g_Z = 13.336$	$g_Z = 13.316$	$g_Z = 13.311$	$g_Z = 13.395$
Anisotropy parameters (D and E)					
$D = 0.045$	$D = 0.085$	$D = 0.073$	$D = 0.043$	$D = 0.079$	$D = 0.067$
$E = 0.010$	$E = 0.016$	$E = 0.014$	$E = -0.008$	$E = 0.000$	$E = 0.000$

model B:

Gd-1		Gd-2	
Basis 1	Basis 2	Basis 1	Basis 2
0.000	0.000	0.000	0.000
0.078	0.294	0.103	0.358
0.212	0.537	0.233	0.610
0.416	0.916	0.439	0.975
g tensor for the ground Kramers doublet (highlighted, pseudospin=1/2)			
$g_X = 1.594$	$g_X = 0.351$	$g_X = 0.952$	$g_X = 0.182$
$g_Y = 4.201$	$g_Y = 0.550$	$g_Y = 1.920$	$g_Y = 0.258$
$g_Z = 11.267$	$g_Z = 13.583$	$g_Z = 12.800$	$g_Z = 13.751$
Anisotropy parameters (D and E)			
$D = -0.021$	$D = 0.067$	$D = -0.025$	$D = 0.068$
$E = -0.016$	$E = 0.017$	$E = -0.015$	$E = 0.022$

model C:

Gd-1		Gd-2	
Basis 1	Basis 2	Basis 1	Basis 2
0.000	0.000	0.000	0.000

0.062	0.140	0.080	0.241
0.176	0.321	0.190	0.415
0.349	0.608	0.360	0.665
g tensor for the ground Kramers doublet (highlighted, pseudospin=1/2)			
$g_x = 1.736$	$g_x = 0.984$	$g_x = 1.058$	$g_x = 0.188$
$g_y = 4.955$	$g_y = 2.010$	$g_y = 2.224$	$g_y = 0.268$
$g_z = 10.686$	$g_z = 12.748$	$g_z = 12.608$	$g_z = 13.741$
Anisotropy parameters (<i>D</i> and <i>E</i>)			
$D = 0.029$	$D = 0.048$	$D = -0.009$	$D = 0.046$
$E = 0.002$	$E = -0.006$	$E = 0.000$	$E = 0.015$

Broken-symmetry Density Functional Theory (DFT) calculation of exchange interaction

We have employed broken-symmetry DFT calculations to explore the exchange coupling between Gd ions within the Gd-EDTA chain. ORCA program package was employed for this scope. The following computational details were employed:

Two structural models were employed, as shown in Figure S19 and S20. The difference between them is that in the larger fragment (S20) the crystallized water molecules in the vicinity of the calculated fragment were included in the calculation. Each fragment was computed within two basis sets: SVP (small-medium) and def2-TZVP (large). B3LYP exchange correlation functional was employed. Scalar relativistic effects were included via the Douglas-Kroll Hess (DKH) Hamiltonian. Other options: VeryTightSCF and Grid7.

In all four cases the calculated exchange coupling was found to be smaller than 0.000 cm^{-1} .

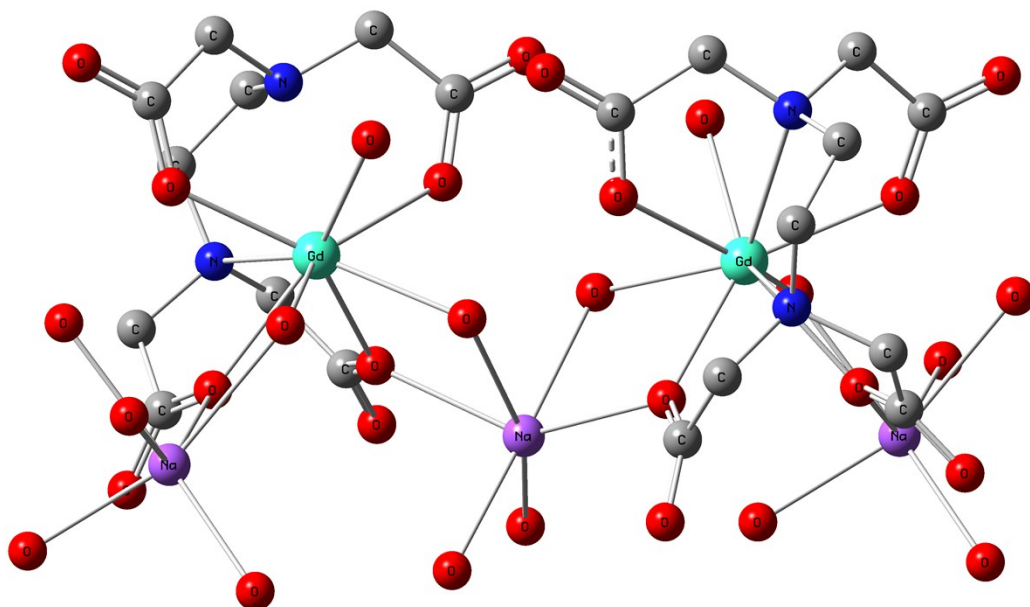


Figure S18. Structure of the calculated binuclear Gd₂ fragment of the Gd-EDTA chain (model D). Hydrogen atoms are not shown for clarity. No crystallized water is included in the calculation.

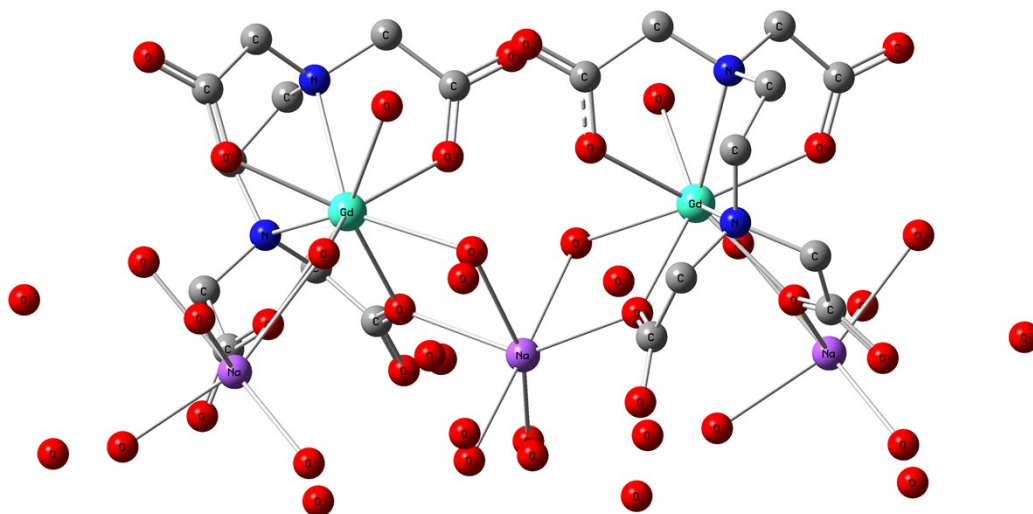


Figure S19. Structure of the calculated binuclear Gd₂ fragment of the Gd-EDTA chain, including the crystallized water molecules included in the calculation (model E). Hydrogen atoms are not shown for clarity.

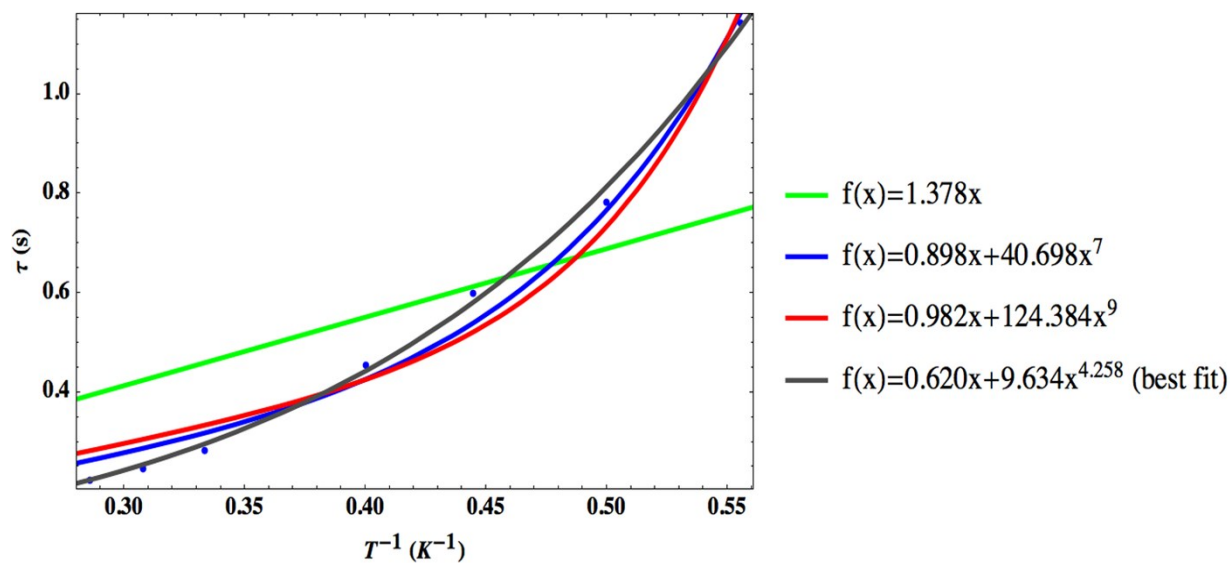


Figure S20. Simulation of temperature dependence of relaxation time for the slow relaxation process (Figure S13). Blue balls are experimental points, lines are simulated dependences with corresponding equations from the right-hand side and $x=1/T$.